Catalysis Science & Technology

Accepted Manuscript

This article can be cited before page numbers have been issued, to do this please use: F. Dai, Z. Li, X. Chen, B. He, R. X. Liu and S. Zhang, *Catal. Sci. Technol.*, 2018, DOI: 10.1039/C8CY01023D.

ROYAL SOCIETY OF CHEMISTRY

rsc.li/catalysis

View Article Online
DOI: 10.1039/C8CY01023D

Synthesis of vanadium phosphorus oxide catalyst promoted by iron-based ionic liquids and its catalytic performance in selective oxidation of n-butane

Fei Dai, Zihang Li, Xuejing Chen, Bin He, Ruixia Liu*, Suojiang Zhang*

Beijing Key Laboratory of Ionic Liquids Clean Process, State Key Laboratory of Multiphase Complex System, Institute of Process Engineering, Chinese Academy of Sciences, Beijing 100190, PR China

ABSTRACT: A series of vanadium phosphorus oxide (VPO) catalysts have been firstly synthesized using iron-based ionic liquids (ILs) as additives for selective oxidation of n-butane to maleic anhydride (MA) in this work. Meanwhile, VPO catalysts doped by inorganic iron salts were also prepared for comparison. The catalytic evaluation presented that iron-based ILs modification remarkably enhanced the n-butane conversion and MA yield. A combination of techniques including XRD, Raman, TG, BET, SEM, TEM, XPS and H_2-TPR were employed to investigate the intrinsic distinction among these catalysts. The results demonstrated that the VPO catalyst promoted by iron-based ILs notably change the catalyst morphology from plate-like structure into chrysanthemum-shape clusters, led to a significant increase in the surface area of the catalyst, and largely promote the formation of $(VO)_2P_2O_7$. All of these were closely associated with the synergistic effect existed between the structure-oriented cation and metal anion in ILs during the preparation of VPO catalyst. In addition, the differences in structure and redox properties of the catalysts studied were also discussed compared with the conventional inorganic salt additives.

Keywords: Vanadium phosphorus oxide; Selective oxidation; n-Butane; Iron-based ionic liquids

Corresponding author: Ruixia Liu, rxliu@ ipe.ac.cn

Suojiang Zhang, sjzhang@ ipe.ac.cn

View Article Online
DOI: 10.1039/C8CY01023D

1. Introduction

Selective oxidation of n-butane to maleic anhydride (MA) is the most successful industrial process for the commercial application of alkane conversion.[1] The vanadium phosphorus oxide catalyst (VPO) with vanadyl pyrophosphate $(VO)_2P_2O_7$ as the main active phase component is considered as the most effective catalyst for this reaction, in which the active phase $(VO)_2P_2O_7$ primarily originates from the topotactic transformation of the precursor $VOHPO_4{\cdot}0.5H_2O$.[2-3] To date, tremendous efforts have been devoted to getting insight into the properties, structure and active phase of the catalysts, etc. However, the VPO catalyst still suffer from many issues, such as small specific surface area (～$20m^2/g$) and low MA selectivity (60～65 mol%), thus the development of efficient VPO catalyst is greatly desired from an economic and environmental point of view.[6-9]

Addition of various metal promoters was usually employed as one effective method to enhance the catalytic behavior of the VPO catalysts by improving n-butane conversion and MA yields.[10,11] VPO catalysts doped by a wide spectrum of metal cations have been widely investigated such as Zn, Bi, Co, Ni, Fe, Cr, Mo, Zr, Nb, Al and Mg, etc.[12-17] Generally, the influences of these dopants are categorized into two major types: structural promoters and electronic promoters.[10] Structural promoters usually were utilized to remove the excess phosphorus and inhibit the formation of undesired phase, while electronic promoters induced electronic changes by replacing V^{4+} and forming the solid solution $[(VO)_{1-x}M_x]_2P_2O_7$. Among these metal promoters, Fe dopant has been viewed to be a typical and efficient promoter. For instance, Sajip et al.[18] pointed out that Fe dopant worked as electronic promoter could affect the re-oxidation of $(VO)_2P_2O_7$ and increase the oxygen mobility. Taufiq-Yap et al.[16] found that the presence of Fe in VPO promoted the activation of the alkane by generation of surface defects to which Lewis acid sites are likely associated, leading to the enhancement in the catalytic activity of VPO catalyst. Other research on incorporation the Fe additive into VPO catalyst were also reported in previous literature.[6,21] In addition, addition of organic structure-directing agent or surfactant in preparation of VPO catalysts could also contribute to the improvement of catalytic performance by modulating the properties of catalyst, such as morphology, specific surface area,

View Article Online
DOI: 10.1039/C8CY01023D

valence state of vanadium, etc. For instance, Carreon et al.[20] have synthesized a macroporous VPO phase with three-dimensional arrays structure of spherical voids employing monodisperse polystyrene sphere arrays as a structure-directing agent, the VPO phase exhibits unprecedented high surface area 75m^2/g and desired macroporous architecture. Guliants et al.[21] proposed that a microporous VPO phase with high surface area (～ 250m^2/g) were prepared by using decyltrimethyl ammonium bromide as surfactant, etc. Inspired by the aforementioned methods, a novel strategy on designing and developing a single compound with dual function of structure-directing agent and Fe promoter is a potential route for the preparation of efficient VPO catalyst.

Recently, ionic liquids (ILs) emerged as important reaction medium or structure-directing agent in inorganic and organic synthesis has attracted much more attentions due to their unique properties such as negligible volatility, good thermal stability, high polarity, strong dissolving ability as well as good recyclability properties, etc.[22-27] Besides, another unique feature of ILs lies in its designable structures that solvents species could be formulated by the modulation and combination of different cations and anions. Therefore, iron-based ILs consist of structure-oriented cations and Fe-metal anions can be designed and synthesized,[28-29] which provide a good opportunity in synthesizing the efficient VPO catalyst. To be best of our knowledge, the IL-assisted synthesis of VPO and its application in selective oxidation of n-butane to MA has never been reported in open literature.

Thus, the objective of this work is attempts to synthesize VPO catalyst promoted by the iron-based ILs for improving the selective oxidation of n-butane to MA, during which the 1-Butyl-3-methylimidazolium Tetrachloroferrate ([BMIM]$FeCl_4$) and 1-Octyl-3-methylimidazolium Tetrachloroferrate ([OMIM]$FeCl_4$) were selected as two typical iron-based ILs. For comparison, VPO catalysts based on the different inorganic iron salts as additives were also prepared and tested in oxidation of n-butane. In addition, the physicochemical properties of the VPO catalysts developed in this work were also systematically examined by a combination of techniques including XRD, Raman, TG, BET, SEM, TEM, XPS and H_2-TPR to further understand the structure-property correlation of sample. This work may provide a new solution for the precise synthesis of VPO catalyst with high n-butane conversion and MA yields.

View Article Online
DOI: 10.1039/C8CY01023D

2. Experimental

2.1 Chemicals and materials

All materials were used without further treatment. Benzyl alcohols (≥99.0%) and phosphoric acid (≥85%) were purchased from Xilong Co., Ltd. Isobutyl alcohol (≥99.0%) was purchased from Tianjin Chemical Reagent Factory. Vanadium pentoxide (≥99.7%) was provided by Handing Co., Lt. The metal precursors, including $Fe(NO_3)_3{\cdot}9H_2O$ and $FeCl_3$, were obtained from Guoyao Chemical Reagent Co, Ltd, China. Metal-based ILs containing [BMIM]$FeCl_4$ and [OMIM]$FeCl_4$, were purchased from Linzhou Keneng Material Technology Co., Ltd, China. The molecular structures of the both iron-based ILs are shown in Fig 1.

2.2 Catalysts preparation

The undoped VPO precursor was usually synthesized using conventional organic method in the following way: V_2O_5 (20g) was refluxed in a mixture of iso-butanol (160 mL) and benzyl alcohol (40 mL) at 135°C for 3 h, then phosphoric acid (15.6 mL, 85 wt. %) was added dropwise to reach a P/V atomic ratio of 1.0 and the mixture was refluxed for another 10 h. After that, the mixture was allowed to cool down to ambient temperature naturally, then the resulting precipitate (light blue solid) was filtered and washed with ethanol to remove the residual reactants. Finally, the catalyst precursor was obtained after drying in oven at 120°C for 12 h.

Four different iron salts were selected as additives for the preparation of Fe-doped catalyst precursors, including $Fe(NO_3)_3{\cdot}9H_2O$, $FeCl_3$, [BMIM]$FeCl_4$ and [OMIM]$FeCl_4$. The preparation method was same as the undoped precursor. Only adding the required amount of iron source (Fe/V molar ratio = 0.02) into the V_2O_5/ alcohol mixture at beginning. The samples obtained are denoted as VPO, VPO-$Fe(NO_3)_3$, VPO-$FeCl_3$, VPO-BMIM$FeCl_4$ and VPO-OMIM$FeCl_4$, respectively.

The catalyst precursors that pressed into pellets and sieved to 20～40 mesh were activated under the initial flow of nitrogen at 400°C for 12h and subsequently continue to be activated under the reaction condition (n-butane/Air=1.4%; GHSV = 2000 h^{-1}) at 420°C for further 24h. After that, the precursors were transformed into the final catalysts.

2.3 Catalysts characterization

The crystallization phase structure of all the catalysts were characterized by using the Rigaku

View Article Online
DOI: 10.1039/C8CY01023D

Ultima IV X-ray diffractometer (XRD) with monochromatized CuKα radiation (λ=0.15418nm) at an emission of 50mA and an accelerating voltage of 40 KV. The patterns were scanned with 2θ ranged from 5° to 90°. The morphologies of the samples were investigated by Hitachi SUB8020 scanning electron microscope (SEM) with an operating voltage of 20KV and by high resolution transmission electron microscope (HRTEM) with the model JEOL JEM-2100 system. The BET surface areas of all catalysts were tested by using N_2 absorption on a micromeritics ASAP 2460 apparatus. The physical properties of the surface of the samples were obtained from X-ray photo electron spectroscopy (XPS, Thermo ESCA Lab-250Xi). All binding energies were corrected with reference to the C1s signal located at 284.6eV. Temperature programmed reduction (TPR) were performed used AutoChem II 2920 with thermal conductivity detector (TCD). All experiments were carried out in a quartz tube of 4 mm diameter with 50 mg sample by raising the temperature from 50 to 900°C at a rate of 10°C min^{-1} under a 5% H_2/Ar mixture flowing at 30 mL min^{-1}. Raman spectra were recorded by using Renishaw UV–vis Raman 1000 system equipped with a CCD detector and a Leica DMLM microscope. The line at 532 nm of Ar^+ laser was used for excitation. The thermogravimetric (TG) analysis was conducted on a TG209F1 thermal analyzer.

2.4 Catalysts testing

The selective oxidation of n-butane was carried out in a fixed-bed flow microreactor with a standard catalyst loading of 4.5g. A mixture of 1.4% n-butane in air was fed to the reactor via calibrated mass flow controller with a gas hourly space velocity (GHSV) of 2000h^{-1}. The test temperature was performed in the range of 380～430°C. The outlet effluents were analyzed by an on-line gas chromatography (GC) with two channels, where the CO, CO_2 was analyzed by a TCD column (molecular sieve 5A (0.6m)) and the n-butane was analyzed by a FID column (30m alumina column substrate). The conversion of n-butane, selectivity of MA and MA yield were calculated by the following equations. The carbon mass balance was typically better than 95%.

$$\text{Conversion of } C_4H_{10} = \frac{C_4H_{10_{in,mol}} - C_4H_{10_{out,mol}}}{C_4H_{10_{in,mol}}} \times 100\%$$

$$\text{Selectivity of MA} = \frac{MA_{out,mol}}{C_4H_{10_{in,mol}} - C_4H_{10_{out,mol}}} \times 100\%$$

$$\text{Yield of MA} = \text{Conversion of } C_4H_{10} \times \text{Selectivity of MA}$$

View Article Online
DOI: 10.1039/C8CY01023D

3. Results and discussion

3.1 Catalyst precursor characterization

The XRD patterns of undoped and Fe-doped precursors are given in Fig. 2, all the patterns are related to the characteristic reflection of vanadyl hydrogen phosphate hemihydrate phase ($VOHPO_4 \cdot 0.5H_2O$) with main peaks appearing at 2θ = 15.7°, 19.8°, 24.3°, 27.2° and 30.6°, corresponding to (001), (101), (021), (121) and (130) planes (Standard card #34-1381), respectively. Any Fe-containing reflections are not detected. The result reveals that the addition of Fe-based ILs has not change the phase structure of precursors. However, all patterns exhibit different intensities and line widths of diffraction peaks, depending on the different iron salts used. The relative peak intensities, full width at half maximum (FWHM) and crystallite size of the (001) and (130) planes calculated by Debye-Scherrer's equation[30] are summarized in Table 1. It is clear that the relative peak intensities of (001) and (130) planes are significantly reduced for all Fe-doped precursors compared to undoped ones, especially for the sample doped with [BMIM]$FeCl_4$ and [OMIM]$FeCl_4$. The same effect was also reported by Sajip et al.,[18] in which the addition of Fe also led to a decrease in the value of $I_{(001)}/I_{(130)}$ of hemihydrate. It has been recognized that the main active plane (020) of $(VO)_2P_2O_7$ will be transformed topologically from the (001) plane of the $VOHPO_4 \cdot 0.5H_2O$ phase,[31,32] thus it is possible to predict that the VPO-BMIM$FeCl_4$ and VPO-OMIM$FeCl_4$ precursors with lowest relative peak intensities $I_{(001)}/I_{(130)}$ is unfavorable in improving the catalytic activity for n-butane oxidation. In addition, there is no obvious change in the FWHM of (001) for all the precursors, indicating that the addition of Fe-based ILs do not cause a decrease in crystallize size of $VOHPO_4 \cdot 0.5H_2O$ phase. Surprisingly, the VPO-BMIM$FeCl_4$ and VPO-OMIM$FeCl_4$ significantly broaden the FWHM of (130) planes from 0.148 to 0.161 and 0.166, respectively, which reduce its crystallize size, while smaller crystallize size in (130) plane is possibly conductive to lattice oxygen mobility to enhance the catalytic performance because the plane is also dominant in $VOHPO_4 \cdot 0.5H_2O$ phase.[33]

The SEM morphology of all the catalysts precursors are presented in Fig. 3. The blank VPO precursor (Fig. 3a) possesses a plate-like crystallite that has a tendency to be arranged into the rosette-shape clusters. The plate-like structure mainly consists of agglomerates of $VOHPO_4 \cdot 0.5H_2O$ platelets that preferentially expose (001) crystal plane.[34] VPO-$Fe(NO_3)_3$

View Article Online
DOI: 10.1039/C8CY01023D

precursor (Fig. 3b) remains the rosette-shape structure with almost same numbers of the platelets. While VPO-$FeCl_3$ precursor (Fig. 3c) is composed of more flat particles with irregular shapes and sizes of the crystallites. Interestingly, the introduction of [BMIM]$FeCl_4$ into VPO precursor leads to the loss of rosette-shape clusters and its plate-like structures are vertical intercrossing onto each other to agglomerate into the chrysanthemum-shape clusters. This special feature can be possibly ascribed to the fact that [BMIM]$FeCl_4$ acting as structure directing agent prevents the growth of crystals in the direction of certain planes and induces growth in particular directions by strong hydrogen bonds interacting with alcohol and phosphate. However, the morphology of VPO precursor exhibits the plate-like structure with smaller crystallite size when using [OMIM]$FeCl_4$ with longer carbon chain as the structure-oriented agent. Based on the above analysis, the incorporation of distinct iron salts in VPO precursor can be observed to significantly influence the morphology of catalysts.

In addition, Fig.4 (a) gives the profiles of thermogravimetric (TG) analysis obtained under the thermal decomposition of blank VPO and VPO-BMIM$FeCl_4$ precursors. Obviously, three different stages in weight loss curves can be observed for both precursors. The first weight loss stage from the room temperature to 200°C mainly attributed to the desorption of the physically adsorbed water, whereas the second step occurring between the 200～440°C originates from the conversion of $VOHPO_4 \cdot 0.5H_2O$ to $(VO)_2P_2O_7$ and the removal of alcohols mixed in the layers of precursor phase. In addition, further weight loss above 440°C may be due to the formation of crystal defects and the progressive dehydration.[35,36] The analysis displays that the both precursors have similar thermal decomposition process, except for a greater weight loss for the second stage of VPO-BMIM$FeCl_4$. To further investigate this phenomenon, a TG profile of blank [BMIM]$FeCl_4$ is recorded in Fig 4(b). The weight loss from 230°C to 500°C may result in the more weight loss in the second stage for VPO-BMIM$FeCl_4$ precursor. A result can be possibly deduced that the removal of [BMIM]$FeCl_4$ as structure-directing agent could increase the specific surface area of the final catalyst and expose more active site. Another distinction in second weight loss step for both catalysts lies in the different final decomposition temperature, of which the VPO-BMIM$FeCl_4$ is 420°C that is 20°C lower than that of blank VPO. This difference is reasonable because the Fe dopant with high lattice oxygen mobility can enhance the oxidation of alcohols at a low temperature.[35]

View Article Online
DOI: 10.1039/C8CY01023D

3.2 n-Butane oxidation studies and catalysts characterization

All precursors were activated in situ in fixed bed reactor and tested as catalysts for selective oxidation of n-butane. Experimental results obtained at 420°C are listed in Table 2. It can be observed that the introduction of Fe salts has a notable influence on the catalytic behaviors of the catalysts. The undoped VPO catalyst exhibits a poor n-butane conversion and MA selectivity, with corresponding to the value of 55.92% and 68.91%, respectively. For VPO-$Fe(NO_3)_3$ and VPO-$FeCl_3$, both the n-butane conversion and MA selectivity are all enhanced under the same reaction conditions compared to the undoped VPO catalyst, attaining the highest selectivity value of 74.16% for VPO-$Fe(NO_3)_3$ catalyst. Surprisingly, the n-butane conversion is remarkably enhanced to 91.6% and 87.77% when using the catalyst VPO-$BMIMFeCl_4$ and VPO-$OMIMFeCl_4$, respectively, yet related MA selectivity is declined to 65.88% and 66.67%. The maximal MA yield of 60.4% was obtained with VPO-$BMIMFeCl_4$ catalyst, which is significantly higher than the MA yield of 38.54% of undoped VPO catalyst.

In addition, the effect of reaction temperature on the n-butane conversion and MA selectivity were also investigated as presented in Fig 5 and 6. The n-butane conversion increase with increasing reaction temperature while the MA selectivity decreases, which can be attributed to the fact that higher reaction temperature result in the overoxidation of MA to carbon oxides. It should be pointed out that the extent of declining in MA selectivity for the catalysts VPO-$BMIMFeCl_4$ and VPO-$OMIMFeCl_4$ is significantly weaker than that of increasing of n-butane conversion compared to blank catalyst, it implied that $[BMIM]FeCl_4$ and $[OMIM]FeCl_4$ are good additives for improving the catalytic performance of VPO in selective oxidation of n-butane to MA.

Subsequently, the characterization of activated catalysts was performed to get insight into the properties, structure and active phase of the catalysts.

Fig. 7 shows the XRD patterns of all the activated catalysts, all the patterns present a well crystallized $(VO)_2P_2O_7$ phase with main peaks at $2\theta = 23^\circ$, 28.6° and 30.1°, which are related to (020), (204), and (221) planes (Standard card #34-1381), respectively. No V^{5+} phase was observed in the XRD profile due to the low content.[37] However, the relative peak intensity and the broadening of the main reflections are quite different for the catalysts with different iron salts. Table 3 also summarizes the relative intensity, FWHM and crystallite size of the (020) and (204)

View Article Online
DOI: 10.1039/C8CY01023D

planes. As shown in Table 3, the various Fe-doped catalysts present the peaks with a lower relative intensity $I_{(020)}/I_{(204)}$ than the undoped sample, in which the ratio of VPO-BMIMFeCl$_4$ is lowest with the value of 0.477. In contrasting with VPO-BMIMFeCl$_4$ catalyst, the use of FeCl$_3$ and [OMIM]FeCl$_4$ lead to a significant increase in the values of $I_{(020)}/I_{(204)}$, indicating the iron sources with different cation could effectively control the morphology, crystallinity and exposure of (020) plane of catalysts. Yet the trends of changes in relative peak intensity for catalysts are in agreement with that of precursors, which further verify the accepted viewpoint that the (001) plane of the VOHPO$_4$·0.5H$_2$O phase could be transformed topologically into active plane (020) of (VO)$_2$P$_2$O$_7$. In addition, the FWHM of patterns are usually used to determine the crystallite size of the catalysts. The thickness of (204) indicates the mean "length" at (204) face, while the thickness of (020) is more representative of the actual thickness.[38] Interestingly, a higher FWHM values and consequently smaller crystallite sizes along the (020) and (204) plane were observed for VPO-BMIMFeCl$_4$ and VPO-OMIMFeCl$_4$ compared with the undoped VPO, VPO-Fe(NO$_3$)$_3$ and VPO-FeCl$_3$, this results fully demonstrated that the use of Fe-based IL as template and additive dramatically affect the formation mechanism and crystalline size of (VO)$_2$P$_2$O$_7$, which is directly associated with catalytic performance in selective oxidation of n-butane to MA.

More information on the crystal structure of the catalysts was measured using the Raman spectra as shown in Fig. 8. The spectrum of pure VPO primarily exhibits four bands at 930, 1016, 1083, and 1181 cm^{-1}, among which the strong bands at 930 and 1181 cm^{-1} are ascribed to the asymmetric P-O-P and V-O-P stretches of (VO)$_2$P$_2$O$_7$, respectively,[39,40] while the weak bands at 1016 and 1083 cm^{-1} can be attributed to δ-VOPO$_4$.[41] The same Raman bands can also be observed for all the Fe-doped catalysts. However, their relative intensities have been remarkably changed. On the one hand, the bands of (VO)$_2$P$_2$O$_7$ for VPO-Fe(NO$_3$)$_3$ and VPO-FeCl$_3$ become distinct and weaker compared to the blank catalyst. In the case of VPO-BMIMFeCl$_4$ and VPO-OMIMFeCl$_4$, the bands intensities are greatly increased, indicating a positive effect of Fe-based ILs addition on the formation of (VO)$_2$P$_2$O$_7$ phase. On the other hand, the significant variation in the band of δ-VOPO$_4$ for VPO-BMIMFeCl$_4$ and VPO-OMIMFeCl$_4$ were not found compared to the blank catalyst. It is generally believed that V^{5+} species usually play an important role in hydrogen abstraction from n-butane, and a synergetic effect of a well-dispersed V^{5+} phase led to enhancement of the n-butane activation and selectivity of MA. G.J Hutchings[42] pointed out

View Article Online
DOI: 10.1039/C8CY01023D

that the addition of Fe additive improved the selectivity to MA, which mainly assigned to the formation of $VOPO_4$ phase.

TEM images shown in Fig. 9 demonstrated clearly the lamellar structure of the obtained VPO-$Fe(NO_3)_3$ and VPO-$BMIMFeCl_4$, and the interplanar spacing is estimated to be around 0.386 nm for VPO-$Fe(NO_3)_3$ and 0.384 nm for VPO-$BMIMFeCl_4$, respectively. It is confirmed that the addition of different iron salts does not cause a drastic change in the crystal structure of $(VO)_2P_2O_7$ but the crystallinity of VPO-$BMIMFeCl_4$ is much better than that of VPO-$Fe(NO_3)_3$ from the electron diffraction patterns, which is in good agreement with XRD patterns.

Table 4 lists the more information on Fe element content, specific surface area, oxidation state of vanadium and atomic ratio of P/V of various catalysts. Similar amount of Fe are doped in VPO-$Fe(NO_3)_3$, VPO-$FeCl_3$, VPO-$BMIMFeCl_4$ and VPO-$OMIMFeCl_4$ catalysts as seen from the ICP analysis, corresponding to the Fe/V atomic ratio of 1.93, 1.94, 1.91 and 1.93×10^{-2}, respectively. Besides, the introduction of different iron salts into VPO catalysts affected the surface area of activated catalysts. Compared with the blank catalyst, doping with $Fe(NO_3)_3.9H_2O$ and $FeCl_3$ slightly reduce the surface area of the catalysts to 13.998 and 13.324 m^2/g, respectively, which is in accordance with the literature.[19] However, BET results demonstrate that the surface areas of catalysts are significantly increased when using the $[BMIM]FeCl_4$ and $[OMIM]FeCl_4$ as structure-directing agent and additives in the synthesis of catalysts, i.e. 30.66 and 22.63 m^2/g. Interestingly, the surface area values are in accordance with the crystallite size of catalyst as shown in Table 1. Obviously, smaller crystallites size shows a higher surface area or vice versa [17]. On this basis, a positive correlation between the surface area with crystallite size of (020) plane of catalyst are presented as shown in Fig. 10.

XPS analysis was performed to investigate the oxidation state of vanadium and surface atomic composition of the catalysts. The oxidation state of vanadium on the surface of VPO catalyst has been a highly controversial issue for the last few years. The results obtained by curve fitting of the spectra in the region of O1s-V2p for blank VPO and VPO-$BMIMFeCl_4$ are shown in Fig. 11. For all catalysts, the curve fitting lead to a single and well-defined binding energy for O1s with value around 531.8ev, while $V2p_{3/2}$ peak can be curve fitted into two peaks with binding energy at 518.5 and 517.5ev, which corresponds to V^{5+} and V^{4+} species, respectively, which is in agreement with the previous studies.[43] The average vanadium oxidation state is subsequently

View Article Online
DOI: 10.1039/C8CY01023D

calculated based on the difference in the binding energy of the O1s and V2$p_{3/2}$ peaks,[44] and the results are summarized in Table 4. It is clearly found that the surface oxidation state of vanadium is decreased and close to V^{4+} for the VPO-BMIM$FeCl_4$ and VPO-OMIM$FeCl_4$ compared to other catalysts, revealing that using the Fe-based ILs as additives in the preparation of VPO catalyst promote the formation of main active phase $(VO)_2P_2O_7$, the variation tendency in surface vanadium oxidation state of catalyst is also accordance with XRD and Raman characterization. In addition, it can be observed from Table 4 that the catalysts VPO-BMIM$FeCl_4$ and VPO-OMIM$FeCl_4$ exhibit higher surface P/V atomic ratios than blank VPO, VPO-Fe$(NO_3)_3$ and VPO-$FeCl_3$, this observation is significant because the excess phosphorous atom is generally believed to be conductive to stabilize the V^{4+} species and inhibit the overoxidation of V^{4+}-containing phase.[16,17]

H_2-TPR analysis was used to investigate the effect of Fe promoters on redox properties. Fig. 12 shows the H_2-TPR profiles of the all catalysts. Blank VPO catalyst displays two reducible peaks at 610 and 761℃, respectively. The former dwarf peak can be attributed to the reduction of lattice oxygen related to V^{5+} phase, whereas the latter strong peak is assigned to the reduction of lattice oxygen associated with V^{4+} phase.[45] Electrical conductivity employed by Herrmann et al. shows that O^- and O^{2-} species are related to V^{4+} and V^{5+}, respectively.[46] The same pattern with two peaks can also be observed for all the Fe-dopant VPO catalysts. However, the relative areas are slightly affected by the additives. An interesting phenomenon from the reduction profile was found that the two peaks for all doped catalysts shift to lower temperature compared to the undoped VPO catalyst, which indicates that addition of different iron salts lead to the enhancement of the reducibility of vanadium valence and thus is beneficial for improvement of the catalytic activity.[35] Also notes that the extent of temperature shift for VPO-BMIM$FeCl_4$ and VPO-OMIM$FeCl_4$ is most notable. The total amount of oxygen removed and ratio for oxygen of V^{5+}/V^{4+} by reduction are calculated and given in Table 5. As observed, the incorporation of the Fe dopant slightly increases the total amount of oxygen removed compared to the blank VPO catalysts with value of 8.763 mmol/g, while VPO-BMIM$FeCl_4$ shows the largest amount of oxygen atoms desorbed with value 10.576 mmol/g, these results further reveal that Fe dopant has a positive ability to enhance the transfer and storage of lattice oxygen. Besides, it is also clear from the Table 5 that the oxygen ratio removed from V^{5+}/V^{4+} decreases with the introduction of Fe

View Article Online
DOI: 10.1039/C8CY01023D

additives, indicating that Fe promotes the formation of $(VO)_2P_2O_7$, this result is also consistent with the Raman and XPS characterization, where the signals of $(VO)_2P_2O_7$ phase are greatly strengthened by the addition of Fe into VPO.

3.3 Discussion

In this work, the different metal iron salts were used as additives to synthesize VPO catalyst based on conventional organic method. All the catalysts promoted by Fe dopant exhibit higher catalytic activity than the blank VPO catalyst. Among the catalysts studied, the catalysts VPO-BMIM$FeCl_4$ and VPO-OMIM$FeCl_4$ doped by Fe-based ILs show the highest MA yields under same reaction conditions, which are notably better than the catalyst VPO-$Fe(NO_3)_3$ and VPO-$FeCl_3$ improved by inorganic iron salts.

Generally, the specific surface area of VPO catalyst has a great impact on the catalytic performance. BET results from the Table 4 have demonstrated that the introduction of [BMIM]$FeCl_4$ and [OMIM]$FeCl_4$ into VPO catalysts significantly enhanced the surface area of activated catalysts compared to the blank VPO catalyst, which lead to the increase in the number of actives sites available for per unit mass of catalyst and cause a remarkable improvement in the n-butane conversion (Table 2). This is also in accordance with the results from the SEM, XRD and TGA analysis. As seen from the Fig. 3 in SEM section, the catalyst VPO-BMIM$FeCl_4$ shows chrysanthemum-shape clusters which differs from the plate-like structure of blank catalyst, this chrysanthemum clusters with regular morphology can expose more space and then is conductive to the increase in the surface area of catalyst. While the catalyst VPO-OMIM$FeCl_4$ greatly reduce the plate size even though the plate-like structure is still observed. Obviously, smaller plate size shows higher surface area or vice versa. XRD analysis as shown in Fig. 7 also further validate the conclusion that both catalyst VPO-BMIM$FeCl_4$ and VPO-OMIM$FeCl_4$ possess smaller crystallite size along the (020) and (204) plane compared to the other catalysts. In addition, TG profile, as observed in Fig. 4, indicated that the decomposition of IL in second weight loss stage also play a positive role in increasing the surface area by generating more gaps in the layer of catalyst. Therefore, using Fe-based ILs as structure-directing agent and promoter in the preparation of VPO notably change the catalyst surface morphology and decline crystallite size, this is a primary influencing factor causing the enhancement of specific surface area. Yet it's worth noting that

View Article Online
DOI: 10.1039/C8CY01023D

there is an obvious distinction in surface area for VPO-BMIMFeCl$_4$ and VPO-OMIMFeCl$_4$ catalysts when adopted Fe-based ILs with different chain long cation as additives, which may ascribe to the fact that the polar functional groups with different transmission properties produced by different ILs change the crystallization rate and formation model of VPO crystal particle by interacting with alcohol and phosphate. In addition, VPO-Fe(NO$_3$)$_3$ and VPO-FeCl$_3$ also show higher n-butane conversion and MA selectivity compared to the blank VPO catalyst (as shown in Table 2), but their specific surface area (i.e. 13.998 and 13.324 m^2/g, respectively) is slightly lower than that of undoped catalyst (14.747m^2/g). These results suggest that the specific surface area of catalyst in this work is not the only factor that affect the catalytic performance.

The phase structure and composition of catalyst also could determine catalytic behavior. As described in XRD, Raman and XPS sections, all the Fe-promoted VPO catalysts have similar phase structures with blank VPO, yet a notable variation in the phase composition can be observed for these catalysts. Raman characterization has shown that the addition of [BMIM]FeCl$_4$ and [OMIM]FeCl$_4$ into VPO promoted the formation of V^{4+} phase, which is in agreement with the results obtained in the XPS and H$_2$-TPR sections. It is generally believed that the $(VO)_2P_2O_7$ phase corresponding to V^{4+} is considered as main active phase of VPO catalyst and the formation of $(VO)_2P_2O_7$ phase is beneficial to enhance the catalytic activity of catalysts.[2,17] From the Fig. 12 in H$_2$-TPR, it also can be seen clearly that the high-temperature reduction peaks for all Fe-doped catalysts shifted to lower temperature compared to the blank VPO catalyst, which indicated that addition of different iron salts enhanced the reducibility of V^{4+} phase and thus improved the catalytic performance. In addition, many literatures have reported that the amount of oxygen species (O^-) linked to V^{4+} are also responsible for the activation of n-butane.[16,46] For instance, the density functional theory (DFT) research made by Hodnetts et. al[47,48] showed that the doubly coordinated oxygen sites P-O-V and oxygen atoms singly coordinated to phosphorous P=O in the $(VO)_2P_2O_7$ (020) surface as selective lattice oxygens indicated a similar local reactivity with respect to electrophilic attacks, the strong nucleophilicity of surface oxygen sites together with the V3d character suggested that the interaction of adsorbate with the $(VO)_2P_2O_7$ (020) surface will lead to the activation of organic species proceeding via to C–H bond splitting. The phosphorous-enriched surface has a higher natural abundance of these P=O oxygen species, which may explain why industrial $(VO)_2P_2O_7$ catalysts generally feature surface-enrichment in

View Article Online
DOI: 10.1039/C8CY01023D

phosphorus.[49-51] Table 5 has demonstrated that the amounts of oxygen species (O^-) for all the Fe-promoted catalysts have been significantly increased. Shen et al.[6] also proposed that Fe-promoted VPO catalysts have more available lattice oxygen and possess higher conversion and selectivity than that of the unpromoted one, which may be attributed to the fact that the introduction of Fe salts improved redox performance of VPO catalysts and increased the activity of oxygen species. Thus the higher amount of oxygen species associated with V^{4+} removed from the Fe-doped catalysts in this work was responsible for the high n-butane conversion and MA selectivity of these catalysts, especially for the catalysts VPO-$Fe(NO_3)_3$ and VPO-$FeCl_3$. On the other hand, Raman and XPS analysis shows that the incorporation of Fe also results in the change of V^{5+} species. However, the role of V^{5+} phase in VPO catalyst is still a controversial issue. Guliants et al.[2] claimed that the V^{5+} phase containing γ and δ-$VOPO_4$ in VPO catalyst are detrimental to their catalytic behavior, while Volta et al.[52] considered that the disorganized δ-$VOPO_4$ phase play an important role in the formation of MA. Centi et al.[53] proposed that the V^{5+} species was responsible for the formation of MA, yet excess V^{5+} species could lead to the overoxidation of MA to COx. A suitable V^{5+}/V^{4+} was suggested to give a high catalytic activity. Therefore, the high catalytic behavior presented by the VPO-$BMIMFeCl_4$ and VPO-$OMIMFeCl_4$ catalysts may be related to its more suitable phase compositions, because the active catalyst for this oxidation reaction requires the coexistence of V^{4+} phase and the appropriate amount of V^{5+} phase.

4. Conclusions

In this work, a series of vanadium phosphorus oxide (VPO) catalysts have been firstly synthesized based on different iron salts as additives for selective oxidation of n-butane to MA. It can be observed that the introduction of Fe dopant has a notably impact on the catalytic behavior. When Fe-based ILs were used as structure-directing agents and promoters, a rather high catalytic performance was obtained, the yield of MA reached up to 60.4% and 58.6% at 420°C for VPO-$BMIMFeCl_4$ and VPO-$OMIMFeCl_4$ respectively, which remarkably higher than that of catalyst VPO-$Fe(NO_3)_3$ and VPO-$FeCl_3$ promoted by inorganic iron salts, whereas lowest catalytic performance was obtained when using the pure VPO catalyst. The characterization results revealed that the VPO catalyst promoted by Fe-based ILs increased the surface area of the catalyst

View Article Online
DOI: 10.1039/C8CY01023D

and changed the catalyst morphology from plate-like structure into chrysanthemum-shape clusters, which led to the enhancement of more active sites. Furthermore, the catalysts VPO-BMIM$FeCl_4$ and VPO-OMIM$FeCl_4$ promoted the formation of $(VO)_2P_2O_7$ and enhanced the available amount of lattice oxygen and reducibility of V^{4+} phase. All of these are suggested to achieve better catalytic performance for selective oxidation of n-butane to MA.

Acknowledgements

This work was supported by National Key Research and Development Program of China (2017YFA0206803), and the Key Programs of the Chinese Academy of Sciences (KFZD-SW-413) and the One Hundred Talent Program of CAS.

References

[1] D. Wang, M. Kung, H. Kung, Catal. Lett., 2000, 65, 9-17.

[2] V. V. Guliants, J. B. Benziger, S. Sundaresan, I. E. Wachs, J. M. Jehng, J. E. Roberts, Catal. Today., 1996, 28, 275-295.

[3] L. K. Leong, K. S. Chin, Y. H. Taufiq-Yap, Catal. Today., 2011, 164, 341-346.

[4] G. J. Hutchings, C. J. Kiely, M. T. Sananes-Schulz, A. Burrows, Catal. Today., 1998, 40, 273-286.

[5] G. J. Hutchings, A. Desmartin-Chomel, R. Olier, J. C. Volta, Nature., 1994, 368, 41.

[6] S. K. Shen, J. P. Zhou, F. S. Zhang, L. Zhou, R. J. Li, Catal. Today., 2002, 74, 37-43.

[7] Y. H. Taufiq-Yap, S. N. Asrina, G. J. Hutchings, N. F. Dummer, J. K. Bartley, J. Nat. Gas. Chem., 2011, 20, 635-638.

[8] X. B. Fan, N. F. Dummer, S. H. Taylor, J. K. Bartleya, G. J. Hutchings, Catal. Today., 2012, 183, 52-57.

[9] G. J. Hutchings, J. Mater. Chem., 2009. 19, 1222-1235.

[10] G. J. Hutchings, R. Higgins, J. Catal., 1996, 162, 153-168.

[11] G. C. Behera, K. M. Parida, D. P. Das, J. Catal., 2012, 289, 190-198.

[12] F. Trifirò, R. K. Grasselli, Top. Catal., 2014, 57, 1188-1195.

[13] G. J. Hutchings, Appl. Catal., 1991, 72, 1-32.

[14] G. C. Behera, K. M. Parida, Catal. Sci. Technol., 2012, 3, 3278-3285.

[15] L. Sartoni, J. K. Bartley, R. P. K. Wells , C. J. Kiely, G. J. Hutchings, J. Mol. Catal. A: Chem., 2004, 220, 85-92

[16] Y. H. Taufiq-Yap, N. M. Nurul Suziana. M. Z. Hussein, Catal. Lett., 2011, 141, 136-148.

[17] H. Y. Wu, H. B. Wang, X. H. Liu, J. H. Li, Appl. Surf. Sci., 2015, 351, 243-249.

[18] S. Sajip, J. K. Bartley, A. Burrows, M. T. Sananes-Schulz, A. Tuel, J. C. Volta, C. J. Kiely, G. J. Hutchings, New. J. Chem., 2001, 25, 125-130.

[19] Y. H. Taufiq-Yap, K. L. Theam, G. J. Hutchings, N. Dummer And J. K. Bartley, Petrol. Sci. Technol., 2010, 28, 997-1012.

[20] S. Dasgupta, M. Agarwal, A. Datta, Micropor. Mesopor. Mat., 2004, 67, 229-234.

[21] M. A. Carreon, V. V. Guliants, Chem. Commun., 2001, 16, 1438.

[22] J. Dupont, J. D. Scholten, Chem. Soc. Rev., 2010, 39, 1780-1804.

[23] J. Łuczak, M. Paszkiewicz, A. Krukowska, A. Malankowska, A. Zaleska-Medynska, Adv. Colloid. Interface. Sci., 2016, 227, 1-52.

View Article Online
DOI: 10.1039/C8CY01023D

[24] Z. He, P. Alexandridis, Phys. Chem. Chem. Phys., 2015, 17, 18238-18261.

[25] J. Łuczak, M. Paszkiewicz, A. Krukowska, A. Malankowska, A. Zaleska-Medynska, Adv. Colloid. Interface. Sci., 2016, 230, 13–28.

[26] K. Yoo, H. Choi, D. Dionysiou, Chem. Commun., 2004, 2000–2001.

[27] Y. Yu, Y. Jiang, M. Tian, L. Yang, H. Yan, S. Sheng, Rare. Metal. Mater. Eng., 2016, 45, 561–566.

[28] R. D. Tilve, M. Varughese Alexander, A. C. Khandekar, S. D. Samant, V. R. Kanetkar, J. Mol. Catal. A: Chem., 2004, 223, 237-240.

[29] M. D. Nguyen, L. V. Nguyen, E. H. Jeon, J. H. Kim, M. Cheong, H. S. Kim, J. S. Lee, J. Catal., 2008, 258, 5-13.

[30] A. L. Patterson, Phys. Rev., 1939, 56, 978.

[31] V. V. Guliants, M. A. Carreon, Catalysis., 2005, 18, 1–45.

[32] H. Igarashi, K. Tsuji, T. Okuhara, M. Misono, J. Phys. Chem., 1993, 97, 7065–7071.

[33] Y. H. Taufiq-Yap, C. K. Goh, G. J. Hutchings, N. Dummer, J. Bartley, Catal. Lett., 2009,130, 327–334.

[34] Y. H. Taufiq-Yap, C. K. Goh, G. J. Hutchings, N. Dummer, J. K. Bartley, J. Mol. Catal. A: Chem., 2006, 260**,** 24–31.

[35] H. Y. Wu, P. Jin, Y. F. Sun, M. H. Yang, C. J. Huang, W. Z. Weng, H. L. Wan, J. Mol. Catal. A: Chem., 2016, 414**,** 1–8.

[36] V. N. Kalevaru, N. Madaan, A. Martin, Appl. Catal. A- Gen., 2011, 391**,** 52–62.

[37] L. K. Leong, K. S. Chin, Y. H. Taufiq-Yap, Appl. Catal. A- Gen., 2012, 415, 53– 58.

[38] Y. H. Taufiq-Yap, C. S. Yuen, R. Irmawati., Chinese. J. Catal., 2014, 35**,** 270–276.

[39] Z. Y. Xue, G. L. Schrader, J. Phys. Chem. B., 1999, 103**,** 9459–9467.

[40] R. M. Feng, X. J. Yang, W. J. Ji, Y. Chen, C. T. Au, J. Catal., 2007, 246**,**166–176.

[41] F. Cavani, S. Luciani, E. D. Esposti, C. Cortelli, R. Leanza, Chem. Eur. J., 2010, 16**,** 1646–1655.

[42] G. J. Hutchings, I. J. Ellison, Catal. Lett., 1996, 38**,** 231-237.

[43] L. Cornaglia, S. Irusta, E. A. Lombardo, M. C. Durupty, J. C. Volta, Catal. Today., 2003, 78**,** 291–301.

[44] X. S. Wang , L. J. Xu, X. Chen, W. J. Ji, Q. J. Yan, Y. Chen, J. Mol. Catal. A: Chem., 2003, 206**,** 261–268.

[45] J. M. Herrmann, P. Vernoux, K. E. B´er´e and M. Abon, J. Catal., 1997, 167, 106–117.

[46] Y. H. Taufiq-Yap, C. K. Goh, G. J. Hutchings, N. Dummer, J. K. Bartley, J, Mol. Catal. A: Chem., 2006, 260**,** 24–31.

[47] D. J. Thompson, I. M. Ciobica, B. K. Hodnett, R. A. van Santen, M. O. Fanning, Surf. Sci., 2003, 547, 438-451.

[48] D. J. Thompson, M. O. Fanning, B. K. Hodnett, J. Mol. Catal. A. Chem., 2003, 206, 435-439.

[49] M. J. Cheng, W. A. Goddard, R. Fu. Top. Catal., 2014, 57, 1171–1187.

[50] M. J. Cheng, W. A. Goddard, J. Am. Chem. Soc., 2013,135, 4600-4603.

[51] W. C. O'Leary, W. A. Goddard, M. J. Cheng, J. Phys. Chem. C., 2017, 121, 24069-24076.

[52] F. B. Abdelouabab, R. Olier, N. Guillaume, F. Lefèbvre, J. C. Volta, J. Catal., 1992, 134**,** 151–167.

[53] G. Centi, F. Trifiro, J. R. Ebner, V. M. Franchetti, Chem. Rev., 1988, 88 , 55–80.

View Article Online
DOI: 10.1039/C8CY01023D

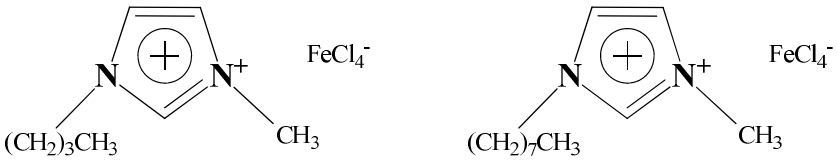

$BMIMFeCl_4$ $OMIMFeCl_4$

Fig. 1 Molecular structure of Fe-based ILs used in this work

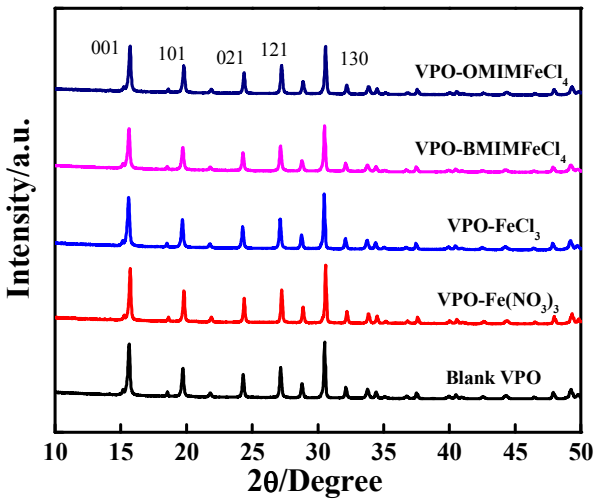

Fig. 2 XRD patterns of Fe-doped and undoped VPO precursors

View Article Online
DOI: 10.1039/C8CY01023D

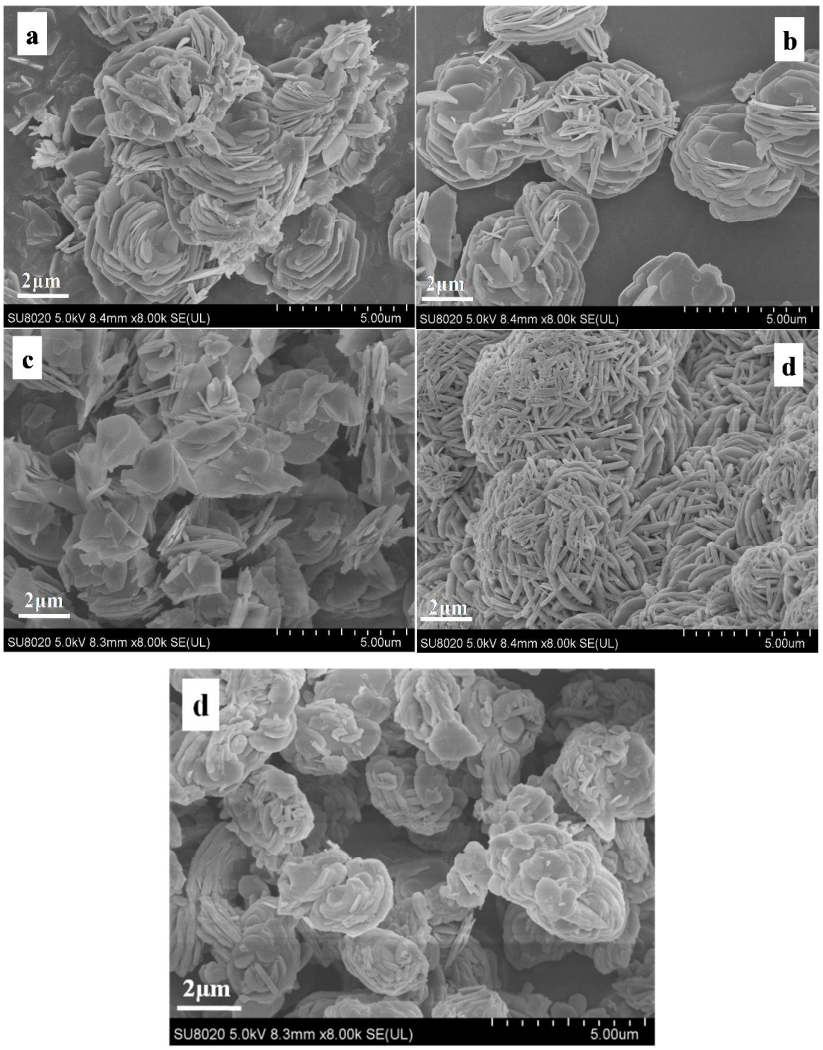

Fig. 3 SEM morphologies of precursors (a) blank VPO (b) VPO-$Fe(NO_3)_3$ (c) VPO-$FeCl_3$ (d) VPO-$BMIMFeCl_4$ (e) VPO-$OMIMFeCl_4$

View Article Online
DOI: 10.1039/C8CY01023D

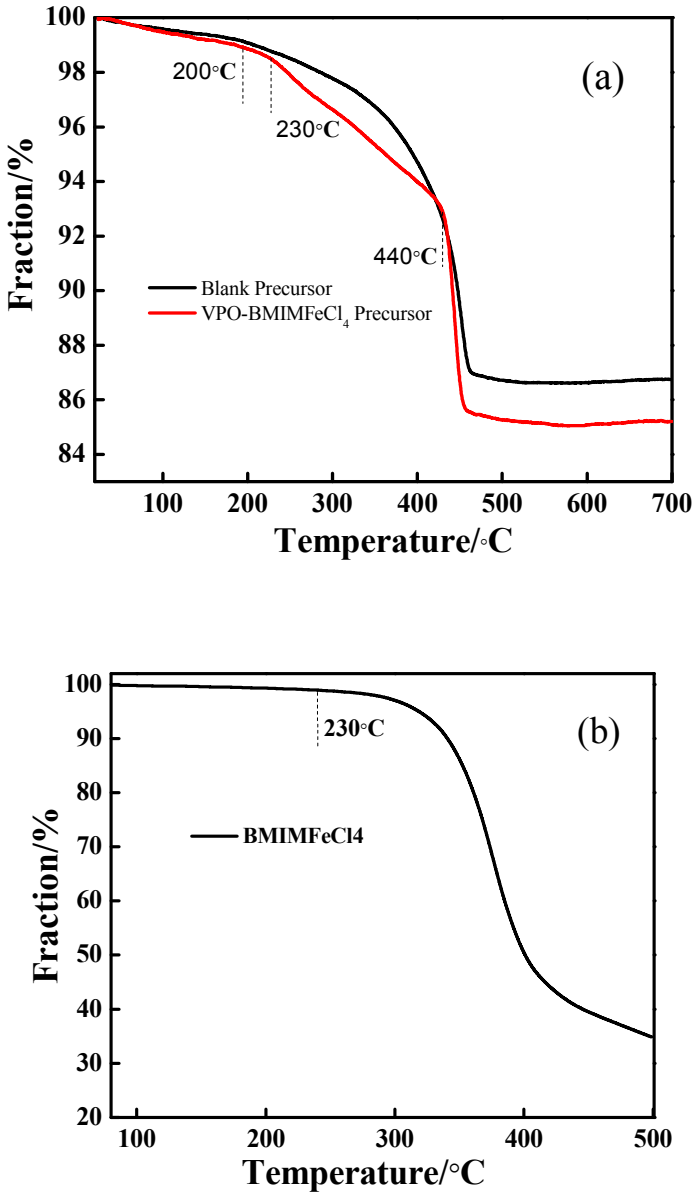

Fig. 4 TG curves of (a) blank VPO and VPO-BMIMFeCl$_4$ precursors (b) [BMIM]FeCl$_4$

View Article Online
DOI: 10.1039/C8CY01023D

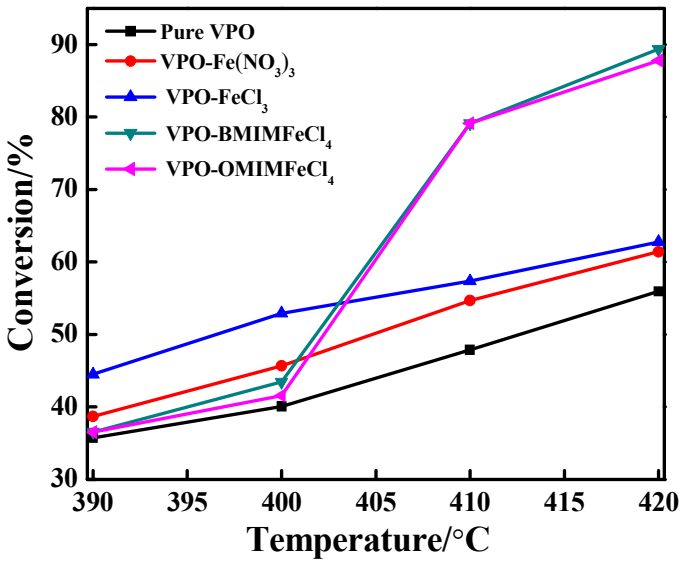

Fig. 5 n-Butane conversion as a function of reaction temperature

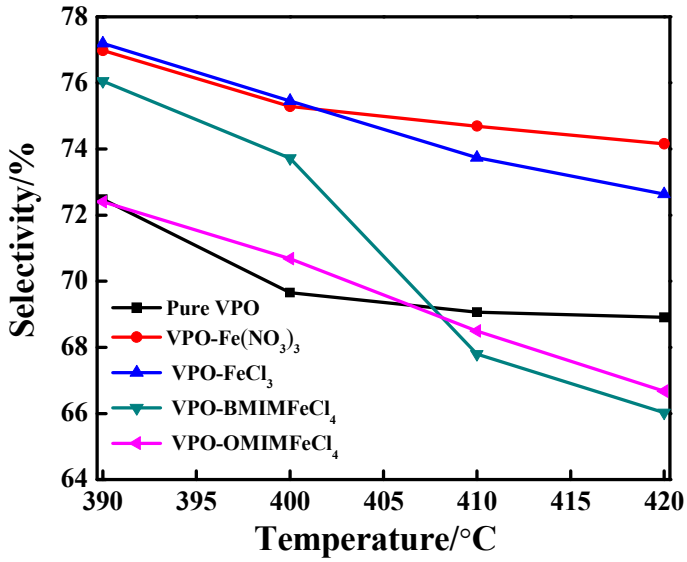

Fig. 6 MA selectivity as a function of reaction temperature

View Article Online
DOI: 10.1039/C8CY01023D

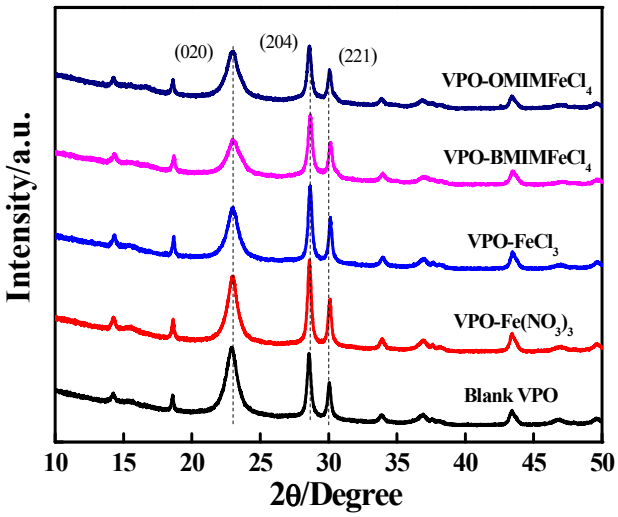

Fig. 7 XRD patterns of Fe-doped and undoped VPO catalysts

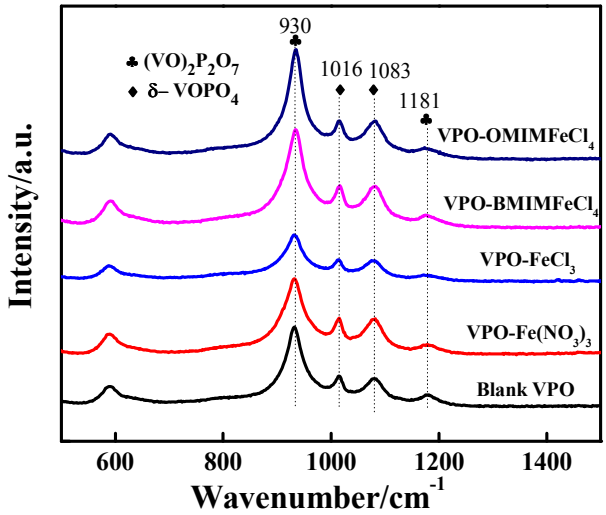

Fig. 8 Raman spectra of Fe-doped and undoped VPO catalysts

View Article Online
DOI: 10.1039/C8CY01023D

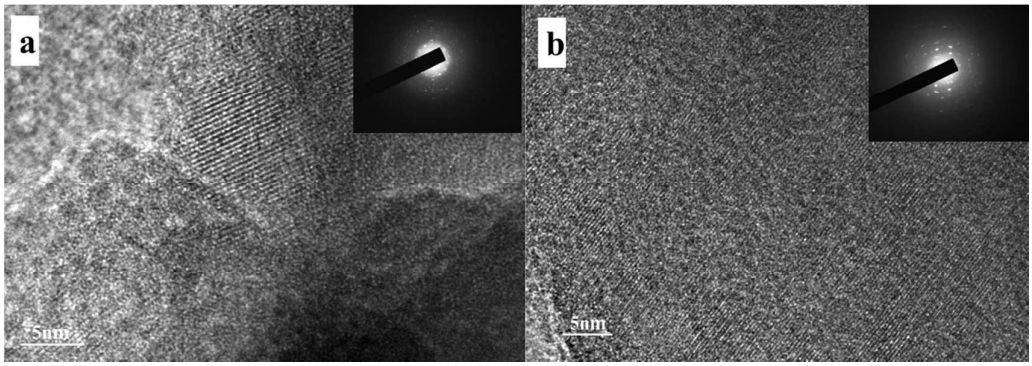

Fig. 9 TEM and electron diffraction patterns (insert) of activated VPO catalysts (a) VPO-$Fe(NO_3)_3$ (b) VPO-$BMIMFeCl_4$

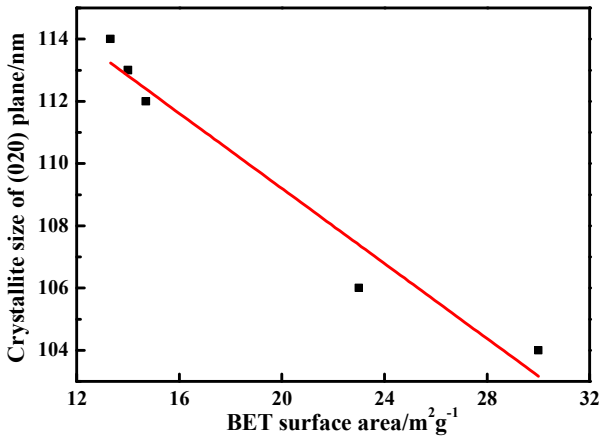

Fig. 10 A correlation between the surface area with crystallite size of (020) plane of catalyst studied

View Article Online
DOI: 10.1039/C8CY01023D

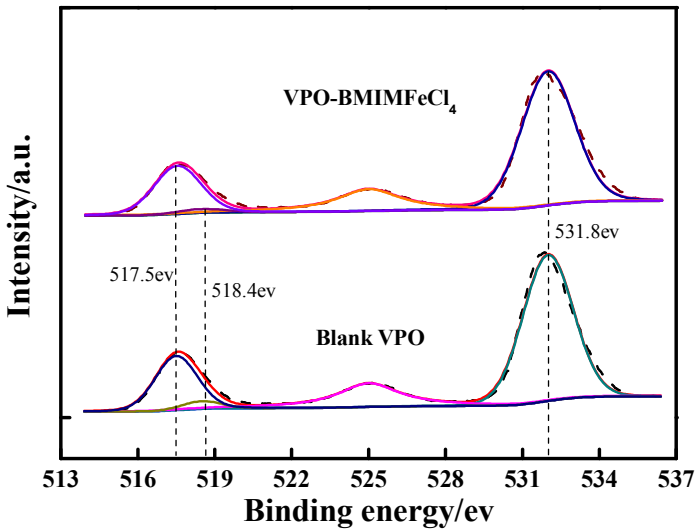

Fig. 11 XPS spectra of O1s-V2p region

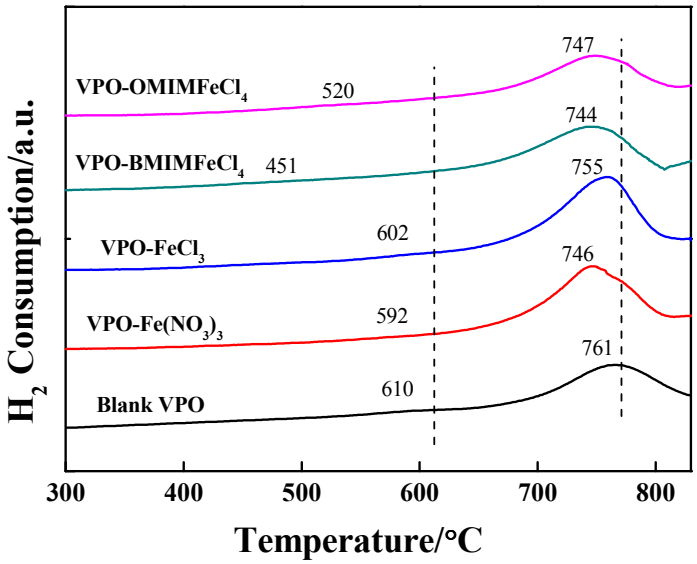

Fig. 12 H_2-TPR profiles of Fe-doped and undoped VPO catalysts

View Article Online
DOI: 10.1039/C8CY01023D

Table 1 XRD data for Fe-doped and undoped VPO precursors

Catalyst	$I_{(001)}/I_{(130)}$	FWHM[a](001)/°	FWHM[b](130) /°	Crystallite size[c](001)/Å	Crystallite size[c](130)/Å
VPO	0.911	0.206	0.148	447	751
VPO-$Fe(NO_3)_3$	0.897	0.204	0.148	452	751
VPO-$FeCl_3$	0.881	0.205	0.149	448	748
VPO-$BMIMFeCl_4$	0.877	0.203	0.161	453	655
VPO-$OMIMFeCl_4$	0.906	0.204	0.166	452	620

[a] Full width at half maximum of (001) reflection for $VOHPO_4 \cdot 0.5H_2O$

[b] Full width at half maximum of (130) reflection for $VOHPO_4 \cdot 0.5H_2O$

[c] Crystallite thickness by means of the Debye-Scherrer's formula[30]

Table 2 Catalytic performance of undoped and Fe-doped VPO catalysts

Catalysts	n-butane conversion (%)	Selectivity (%)			$Yield_{MA}$(%)
		MA	CO	CO_2	
Blank-VPO	55.92	68.91	20.04	11.06	38.54
VPO-$Fe(NO_3)_3$	61.42	74.16	17.06	8.77	45.55
VPO-$FeCl_3$	62.75	72.64	18.90	8.46	45.58
VPO-$BMIMFeCl_4$	91.6	65.88	22.53	11.59	60.4
VPO-$OMIMFeCl_4$	87.77	66.67	22.54	10.79	58.52

Conditions: T=420°C, GHSV=2000h^{-1}, C_4H_{10}/Air=1.4/98.6.

View Article Online
DOI: 10.1039/C8CY01023D

Table 3 XRD data for Fe-doped and undoped VPO catalysts

Catalyst	$I_{(020)}/I_{(204)}$	FWHM[a](020)/	FWHM[b](204) /°	Crystallite size[c](020)/Å	Crystallite size[c](204)/Å	Interplanar spacing (020) /Å
VPO	0.899	0.728	0.340	112	252	3.884
VPO-$Fe(NO_3)_3$	0.699	0.716	0.341	113	252	3.867
VPO-$FeCl_3$	0.575	0.727	0.333	115	258	3.879
VPO-$BMIMFeCl_4$	0.477	0.785	0.366	104	233	3.855
VPO-$OMIMFeCl_4$	0.742	0.774	0.356	106	241	3.857

Table 4 Characterization data of catalysts

Catalyst	Surface Area (m^2/g)	$Fe/V \times 10^2$	$V2p_{3/2}$	O1s	Vox	P/V
Blank VPO	14.747	-	517.69	531.97	4.11	1.65
VPO-$Fe(NO_3)_3$	13.998	1.93	517.61	531.86	4.13	1.67
VPO-$FeCl_3$	13.324	1.95	517.44	531.71	4.12	1.68
VPO-$BMIMFeCl_4$	30.661	1.91	517.61	531.94	4.07	1.71
VPO-$OMIMFeCl_4$	22.627	1.93	517.35	531.66	4.09	1.70

Using the following correlation: $Vox=13.82-0.68[O1s-V2p_{3/2}]$[44]

View Article Online
DOI: 10.1039/C8CY01023D

Table 5 Total amounts of oxygen atoms removed and ratio for oxygen removed of V^{5+}/V^{4+} by H_2/Ar

Catalyst	T/°C	O atoms removed /mmol/g	Ratio for oxygen removed from V^{5+}/V^{4+}
Blank-VPO			
1	610	0.175	0.020
2	761	8.588	
Total oxygen atoms desorbed		8.763	
VPO-Fe$(NO_3)_3$			
1	592	0.016	0.0017
2	746	9.393	
Total oxygen atoms desorbed		9.409	
VPO-$FeCl_3$			
1	602	0.119	0.0118
2	755	10.125	
Total oxygen atoms desorbed		10.244	
VPO-BMIM$FeCl_4$			
1	451	0.106	0.0101
2	744	10.470	
Total oxygen atoms desorbed		10.576	
VPO-OMIM$FeCl_4$			
1	520	0.066	0.0076
2	747	8.675	
Total oxygen atoms desorbed		8.741	

View Article Online
DOI: 10.1039/C8CY01023D

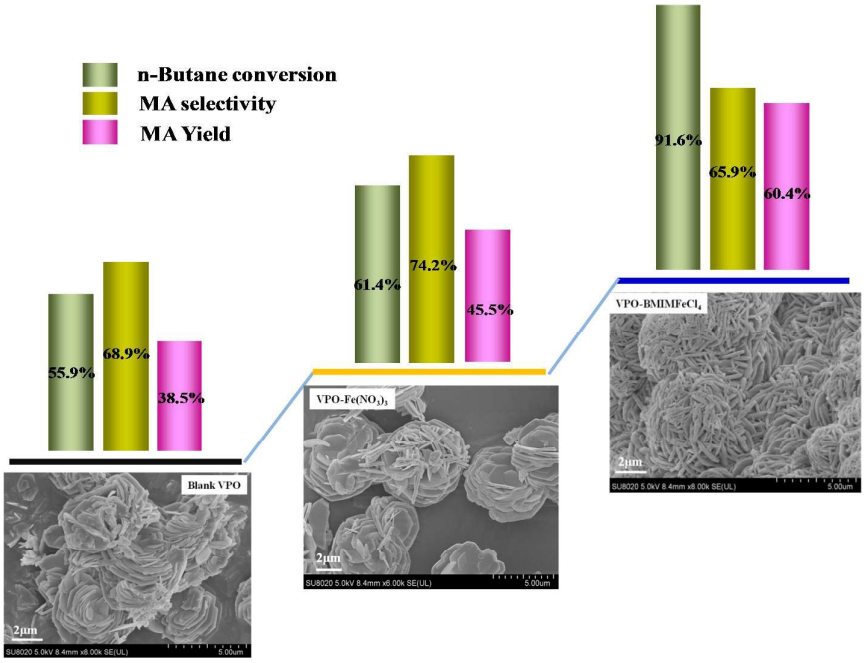

Catalytic performance of undoped and Fe-doped VPO catalysts